† Electronic Supplementary Information (ESI)

Boosting catalytic performance of graphene-supported Pt nanoparticles via decorating with -$SnBu_n$: an efficient approach for aqueous hydrogenation of biomass-derived compounds

Adrián García-Zaragoza,[a] Christian Cerezo-Navarrete,[a,] Pascual Oña-Burgos[a] and Luis M. Martínez-Prieto[a,b,*]*

[a] ITQ, Instituto de Tecnología Química, Universitat Politècnica de València (UPV), Av. de los Naranjos S/N 46022, Valencia, Spain

[b] IIQ, Instituto de Investigaciones Químicas (CSIC-Universidad de Sevilla), Departamento de Química Inorgánica; Avda. Americo Vespucio 49, 41092, Sevilla, España.

E-mails: chcena@posgrado.upv.es; luismiguel.martinez@csic.es

Table of Content

S1. Experimental Part

1.1. General considerations and starting materials

Most chemical operations were carried out under nitrogen atmosphere using conventional Fischer-Porter bottles, Schlenk technique or in a glovebox. THF (Sigma-Aldrich) was purified before use by distillation under argon atmosphere through filtration in the column of a solvent purification system (SPS). The organometallic platinum precursor, $Pt(NBE)_3$ [NBE = norbornene], was purchased from Nanomeps (Toulouse), rGO from Graphenea, and the commercial products Bu_3SnH (97 %), vanillin (99 %), levoglucosenone (> 95 %), furfural (99 %), levunilic acid (98 %) and dodecane (99 %) from Merck. The biomass-derived substrate, 5-hydroxymethylfurfural (HMF, 97 %) was purchased from Carbosynth. All reagents were used without prior purification, except for HMF and furfural which were purified by filtering with an equimolar silica:alumina mixture, and stored in a refrigerator.

Transmission Electron Microscopy (TEM) and High-Resolution TEM (HRTEM). **Pt@rGO/Sn$_x$** (x = 0, 0.2, 0.5, 0.8 and 1 equiv.) and **Pt/Sn$_2$** NPs were analyzed by TEM and HRTEM, after the deposition on a copper grid a drop of a suspension of them in THF. TEM and HRTEM analyses were performed at the "Servicio de Microscopia Electrónica" of Universitat Politècnica de València (UPV). TEM equipment consists in a JEOL JEM 1400Flash electron microscope operating at 120 kV with a point resolution of 3.8 Å. The size distribution of the nanoparticles was performed with ImageJ software by measuring numerous particles on a given grid. HRTEM analysis were performed with a JEOL JEM 2100F electron microscope operating at 200 kV with a resolution point of 2.35 Å, both in transmission (TEM) and scanning-transmission modes (STEM) using a dark-field detector (DF). FFT (Fast Fourier Transform) treatments have been carried out with DigitalMicrograph software version 3.7.4.

Inductively Coupled Plasma Optical Emission Spectrometry (ICP-OES). Digestion of supported and non-supported Pt NPs were performed following a method recently reported.[1] Specifically, *ca.* 30 mg of catalyst sample were suspended in 21 mL solution of HCl:HNO_3 (6:1) and, then, sonicated for 90 minutes. After that, the samples were digested at 180 °C for 15 hours and, finally, the solution was cooled down to room temperature, diluted with 100 mL of deionized water and analyzed by ICP. The ICP-OES analysis were carried out at the technique service of the "Instituto de Tecnología Química (ITQ)", using a Varian 715-ES equipment.

Raman spectroscopy. Raman spectra were recorded using an excitation wavelength of 514 nm were set in a Renishaw in Via Raman spectrometer equipped with a Lyca microscope. The reduced graphene oxide (rGO) and rGO-supported Pt NPs (powder) were deposited in an Al support, and measured within the region of 0 to 3000 cm^{-1} with a resolution of < 4 cm^{-1}.

Diffuse Reflectance Infrared Fourier Transform spectroscopy (DRIFT). DRIFT measurements were carried out on a Bruker Vertex 70 equipment with a 3 mm aperture, 20 KHz speed and a resolution of 4 cm^{-1}. DRIFT analysis of **Pt/Sn$_2$** was performed by preparing a suspension of the catalyst in THF. Then, a drop of this dispersion, before and after bubbling CO for 5 minutes, was added on a sample holder with KBr located in the cell of the equipment.

X-Ray Photoelectron Spectroscopy (XPS). XPS analyses of **Pt@rGO/Sn$_x$** (x = 0, 0.2, 0.5, 0.8 and 1 equiv.) and **Pt/Sn$_2$** were performed using a SPECS device equipped with a Phoibos 150-9MCD detector using Al-Kα radiation (hυ=1483.6 eV) with a pass energy of 30 eV. The pressure during the analysis was kept under

10^{-9} Torr. The quantification and evaluation of the spectra has been carried out with the help of the *CASA* software, referencing them in base of C1s = 284.5 eV.

X-ray powder diffraction (XRD). XRD analysis was performed with the help of a PANanlytical CubiX diffractometer using Cu-Kα (1.5406 Å) radiation equipped with an autosampler. XRD measurement for **Pt/Sn_2** was performed under inert atmosphere, depositing the NPs in the centre of a specially designed sample holder for unstable samples sealed with a Kapton foil inside a glove-box. On the other hand, **Pt@rGO/$Sn_{0.8}$** was measured in a sample holder together with grease to secure the sample.

H_2 and CO chemisorption. H_2 and CO adsorption measurements were performed using the double isotherm method on a Quantachrome Autosorb-1C equipment. For both measurements, no prior activation of the catalyst was performed, at high temperatures a chemical transformation in the catalysts can occur and maybe form PtSn alloys, as was previously observed.[2] First, the samples were degassed at $1333 \cdot 10^{-3}$ Pa for 2 h under a stream of He. Then, pure H_2 or CO at 25 °C was admitted and the first adsorption isotherm was measured. After evacuation at 25 °C, the second isotherm was taken. The amount of chemisorbed H_2 or CO was then obtained by subtracting the two isotherms (V_m). The pressure range studied was $0.5\text{-}11 \cdot 10^4$ Pa. The dispersion of Pt was calculated from the amount of irreversibly adsorbed H_2 assuming a stoichiometry of Pt/H = 1 (Equation 1).

The chemisorption uptake expressed in micromoles of hydrogen or carbon monoxide per gram of sample is calculated as:

$$N_m = 44.61 \cdot V_m \quad (Equation\ 1)$$

where N_m is the number of adsorbed gas molecules (expressed as μmol/g), and V_m is the volume required to fill a monolayer of adsorbed gas. On the other hand, the metal dispersion, D, is defined as the fraction of metal atoms found on the surface of active metal particles and it is expressed as a percentage of all metal atoms present in the sample.

$$D = \frac{N_m \cdot S \cdot M}{100 \cdot L} \quad (Equation\ 2)$$

where M and L are the molecular weight and percent loading (in our case ~3 wt%) of the supported metal, and S the stoichiometry assumed of Pt/H = 1.

Temperature-programmed reduction (TPR). For the catalyst characterization a Micromeritics AutoChem 2910 system with a thermal conductivity detector (TCD) was used. No prior activation of the catalyst was performed. First, about 40 mg of the sample was treated at room temperature in flowing He (10 mL/min) for 20 min to degas the sample. Then, the sample was heated from 25 to 600 °C with a rate of 5 °C/min in a flow of 10 vol% H_2 in Ar. The total gas flow rate was 50 mL/min.

Temperature-programmed desorption (TPD). TPD-H_2 studies were performed using a quartz reactor connected online to a mass spectrometer Balzer (QMG 220M1). For the measurement of the unmodified and functionalized catalyst (**Pt@rGO** and **Pt@rGO/$Sn_{0.8}$**, respectively), no prior activation was needed. Specifically, 50 mg of the sample was degassed at room temperature in a flow of 10 vol% H_2 in Ar (20 mL/min) during 1 h. After the adsorption, the temperature was increased to 600 °C (10 °C /min), maintaining the Ar flow. H_2 desorption was followed by MS.

Gas Chromatography (GC). The chromatograms of substrates and different products obtained were recorded with a Varian CP-3800 equipped with an automatic injector Varian CP-8400 and a suprawax column. The method used starts with an injection temperature of 50 °C. After hold the temperature for 1 minute, the column is heated to a 240 °C (20 °C/min) maintaining this temperature 3.5 minutes. For the GC measurements of water-based samples, a 200 µL of the sample was diluted with 800 µL isopropanol with 0.1 mmol of dodecane (used as standard).

Gas Cromatography-Mass Spectrometry (GC-MS). GC-MS analyses were carried out in an Agilent 6890N chromatograph equipped with a HP-5 column (30 m, 0.32 mm, 0.25 µm), coupled to an Agilent 5973N electron impact mass spectrometer.

1.2. Synthesis of graphene-supported Pt NPs and non-supported Pt NPs

Pt@rGO. This material was prepared following a previously reported synthetic method.[2] More specifically, a Schlenk flask was charged with 8 mg (0.017 mmol) of $Pt(NBE)_3$ and dissolved in 3 mL of anhydrous and deoxygenated THF. After that, the solution was added to a 100 mL Fischer-Porter bottle with a suspension of 100 mg of reduced graphene oxide (rGO) in 50 mL of THF, previously sonicated during 60 min. The Fischer-Porter was then pressurized with 3 bar H_2 and the dispersion was stirred vigorously during 20 h at room temperature. After that, the pressure was released and **Pt@rGO** was filtered through a polyamide membrane (Whatman® membrane filters, 47mmx0.45µm) under vacuum and washed with 50 mL of THF. Finally, the catalyst was dried overnight in an oven at 60 °C. The nanoparticle size was measured by TEM on a population of at least 100 NPs, which afforded a mean value of 2.3 ± 0.7 nm. ICP measurements gave a Pt content of 2.55 wt%.

Pt@rGO/$Sn_{0.2}$. This Sn-functionalized catalyst was synthesized following a two-step synthetic route. First, **Pt@rGO** was synthesized as described above. Then, before the purification and just after the H_2 pressure was released, a solution of the organometallic tin complex Bu_3SnH (0.003 mmol, 1 mg) in 2 mL of THF was added. This dispersion was stirred overnight, and the resulting **Pt@rGO/$Sn_{0.2}$** was filtered through a polyamide membrane (Whatman® membrane filters, 47mmx0.45µm) under vacuum and washed with 50 mL of THF. Finally, the black precipitate was dried overnight in an oven at 60 °C. The nanoparticle size was measured by TEM on a population of at least 100 NPs, which afforded a mean value of 2.3 ± 0.5 nm. ICP measurements gave a total metal content of 2.61 wt%, which corresponds to a 2.38 wt% Pt and 0.23 wt% Sn.

Pt@rGO/$Sn_{0.5}$, **Pt@rGO/$Sn_{0.8}$** and **Pt@rGO/Sn_1** were prepared as described for Pt@rGO/$Sn_{0.2}$, but adding different amounts of Bu_3SnH. For more information, see Table S1.

Pt/Sn_2. A Schlenk flask was charged with Bu_3SnH (122 mg, 0.419 mmol, 2 equiv.) and dissolved in 10 mL of deoxygenated and anhydrous THF from the SPS. After that, the solution was added to a 100 mL Fischer-Porter bottle charged with a cooled solution (-80 °C) of $Pt(NBE)_3$ (100 mg, 0.209 mmol) in 25 mL of THF (previously degassed by three freeze-pump cycles). The Fischer-Porter was then pressurized with 3 bar of H_2, and the solution was allowed to reach room temperature while the solution was stirred vigorously. A black homogeneous solution was formed, and the stirring was kept for 20 hours at room temperature. After that, the remaining H_2 pressure was released with vacuum, and 50 mL of anhydrous pentane was added to the solution to favour the precipitation of **Pt/Sn_2** NPs,. Finally, the resulting Pt NPs were dried overnight under vacuum. The size of the NPs was measured by TEM image on a sample of a least 100 nanoparticles,

which afforded a mean value of 1.6 ± 0.5 nm. ICP measurements gave a total metal content of 83.9 wt%, which corresponds to a 49.2 wt% Pt and 34.7 wt% Sn.

Pt/Sn_2@rGO. It consists in a two-step synthetic procedure. First, **Pt/Sn_2** NPs were prepared as described before. In a second step, 6 mg of **Pt/Sn_2** NPs (49.2 wt% and 34.7 wt% Sn) was added to a Fischer-Porter bottle previously charged with a suspension of rGO (100 mg) in 50 mL THF. After 24 h of vigorous stirring, Pt/Sn2 NPs were adsorbed on the rGO and the resulting **Pt/Sn_2@rGO** was filtered through a polyamide membrane (Whatman® membrane filters, 47mmx0.45µm) under vacuum and washed with 50 mL of THF. Finally, the black precipitate was dried overnight in an oven at 60 °C. The nanoparticle size was measured by TEM on a population of at least 100 NPs, which afforded a mean value of 1.5 ± 0.3 nm. ICP measurements gave a total metal content of 4.3 wt%, which corresponds to a 2.52 wt% Pt and 1.78 wt% Sn.

Table S1. Summary with the synthetic information of the different catalysts based on Pt NPs.

Catalyst	$Pt(NBE)_3$ (mmol)	Bu_3SnH (mmol)	TEM size (nm)	ICP (wt%)	Sn/Pt
Pt@rGO	0.017	-	2.3 ± 0.7	Pt: 2.55 Sn: -	-
$Pt@rGO/Sn_{0.2}$	0.017	0.003	2.3 ± 0.5	Pt: 2.38 Sn: 0.23	0.16
$Pt@rGO/Sn_{0.5}$	0.017	0.008	2.3 ± 0.4	Pt: 2.56 Sn: 0.28	0.18
$Pt@rGO/Sn_{0.8}$	0.017	0.013	2.1 ± 0.5	Pt: 2.51 Sn: 0.40	0.26
$Pt@rGO/Sn_1$	0.017	0.017	2.4 ± 0.5	Pt: 2.49 Sn: 0.50	0.33
Pt/Sn_2	0.209	0.419	1.6 ± 0.5	Pt: 49.2 Sn: 34.7	1.15
Pt/Sn_2@rGO	-	-	± 0.3	Pt: 2.52 Sn: 1.78	1.16

1.3. Determination of butane by analysis of the reaction sky

To detect the existence of butane in the reaction sky, we synthesized **$Pt@rGO/Sn_{0.8}$** and **Pt/Sn_2** in the same way as described above. Once the synthesis of the catalysts were performed but the Fischer-Porter was still pressurized, we took an aliquot of 50 µL of the reaction sky and analyzed it in an Agilent 8890 GC equipped with a DB-1 column and a FID detector. The retention time of butane was previously determined using commercial butane (98 %, Merck).

1.4. Catalytic hydrogenation reactions

The hydrogenation of biomass-derived oxygenated substrates (i.e. HMF, furfural, vanillin, levoglucosenone and levulinic acid), were performed in a 5 mL reactor equipped with a magnetic stirring bar (750 rpm) and filled with the rGO-supported Pt NPs (2 mg, 0.0003 mmol Pt). Then, the corresponding substrate (0.2 or 0.3 mmol) and anhydrous THF or deionized water (2 mL) were added before the air atmosphere of the vial

was exchanged by carefully pressurizing/depressurizing the reactor with hydrogen three times. After pressurizing at 5 bar H_2, the reaction mixture was stirred at room temperature (in an oil bath at 25 °C) for 5 h. Finally, the catalyst was separated by filtration, and the reaction mixture was analyzed by GC and GC-MS using dodecane as standard.

Calculation of conversions and selectivities:

In all cases, the calibration was done using dodecane as internal standard. The response factor of the analytes (RF_i) was determined by injecting known quantities of each analyte *i* into the corresponding GC:

$$mol_i = \frac{A_i}{A_{PI}} \cdot \frac{mol_{PI}}{RF_i}$$

being A_i the area of the analyte, A_{PI} the area of the standard (dodecane) and mol_{PI} the exact mol of the standard added. Thus, conversions and selectivities were calculated as follows:

$$Conversion = \frac{mol_{product\ i}}{\sum mol_{products}}$$

Carbon balance was obtained as follows, reaching carbon balance values greater than 95 % in all cases:

$$\%\ Carbon\ balance = \frac{mol_{HMF} + mol_{BHMF} + mol_{others}}{mol_{HMF\ initial}}$$

The catalyst turnover frequencies (TOF, h^{-1}) were expressed as the ratio moles of converted substrate (HMF) and bulk catalyst (in order to compare) as a function of time:

$$TOF\left(h^{-1}\right) = \frac{mol_{HMF}/mol_{bulk\ catalyst}}{time}$$

1.5. Kinetic experiments

For the kinetic experiments, the reactor was charged and pressurized at the corresponding reaction conditions, and aliquots of 200 µL were taken from the reaction medium each hour. Then, aliquots were analyzed by GC, using dodecane as internal standard. Except for the aqueous reactions, where the aliquots were diluted in 800 µL isopropanol.

1.6. Multiple Addition Experiment

For the multiple addition experiment, the reactor was charged and pressurized at the reaction conditions [0.3 mmol HMF, 2 mg **Pt@rGO/Sn$_{0.8}$** (0.1 mol% Pt), 25 °C, 5 bar H_2, 2 mL deionized water]. Each hour, an aliquot was taken from the reaction medium and new substrate (i.e. HMF) was added to the reactor. The aliquots were analyzed by GC using dodecane as standard, and confirmed by GC-MS.

1.7. Filtration experiment

For this experiment, the reactor was charged and pressurized at the reaction conditions [0.3 mmol HMF, 2 mg **Pt@rGO/Sn$_{0.8}$** (0.1 mol% Pt), 25 °C, 5 bar H_2, 2 mL deionized water]. After 1 h reaction, **Pt@rGO/Sn$_{0.8}$**

was removed by filtration, and another clean and empty reactor was charged with the mother liquor solution under the same reaction conditions. Then, the conversion of HMF was determined after 2 and 4 h and compared to the reaction where the catalyst was not filtered (see Figure 4b). No change in the conversion was observed. After the filtration, the mother liquor solution was analyzed by ICP, giving a metal content negligible (< 0.1 ppm).

1.8. UV-vis adsorption HMF/BHMF experiments

To calculate the adsorption of HMF/BHMF on **Pt@rGO** and **Pt@rGO/$Sn_{0.8}$** catalysts, we first made a calibration with different concentrations of HMF and BHMF (see SI section S16, Figures S28 and S29) in order to determine their respective absorptivity coefficients (ε) by the Beer-Lambert equation:

$$A = \varepsilon \cdot l \cdot C$$

where A is the absorbance, l optical path length and C the concentration of the substrate. Once ε has been calculated, we prepared a 10 mg/L (ppm) solution of HMF and BHMF to which we added 1mg/10 mL of the corresponding catalyst (**Pt@rGO** and **Pt@rGO/$Sn_{0.8}$**). We left it under constant stirring for 20 h, and proceeded to determine the absorbance value of the solution after filtering the catalyst under study. Interpolating, we are able to obtain the concentration (ppm) of substrate remaining in the solution, and, therefore, the amount of HMF or BHMF adsorbed by the catalyst (mg/g_{cat}).

S2. Butane analysis of reaction atmosphere

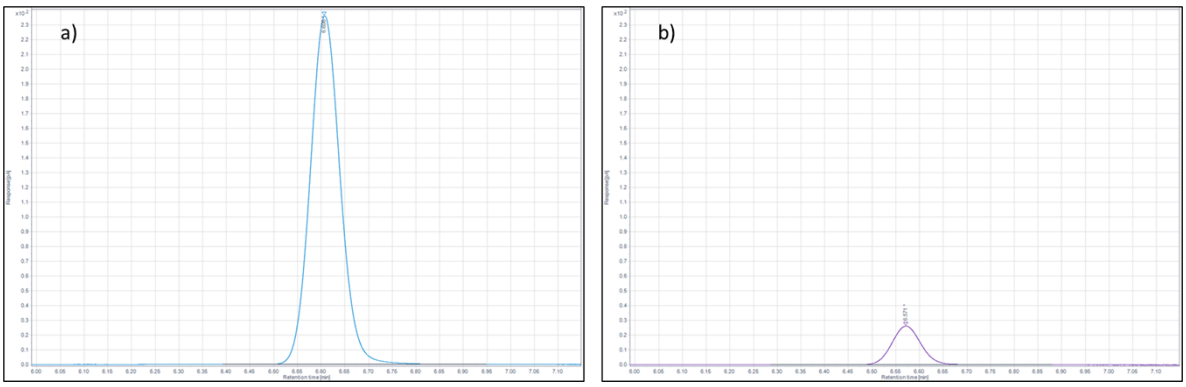

Figure S1. GC chromatogram revealing the butane released into the atmosphere during the synthesis of **Pt/Sn_2** (a, blue line) and **Pt@rGO/$Sn_{0.8}$** (b, purple line).

S3. ICP-AES and STEM-EDX

Table S2. ICP-AES and STEM-EDX analysis for **Pt@rGO/Sn$_x$**.

Catalyst	Pt wt%[a]	Sn wt%[a]	n_{eq} Sn[b] ICP	n_{eq} Sn[c] EDX	%Pt_{surf} atoms	Pt_{surf}/Sn[d]
Pt@rGO	2.55	-	-	-	47.7	-
Pt@rGO/$Sn_{0.2}$	2.38	0.23	0.16	0.12	47.7	3.00
Pt@rGO/$Sn_{0.5}$	2.56	0.28	0.18	0.17	47.7	2.65
Pt@rGO/$Sn_{0.8}$	2.51	0.40	0.26	0.22	51.3	1.96
Pt@rGO/Sn_1	2.49	0.50	0.33	0.27	46.0	1.39

[a] % of Pt and Sn obtained by ICP-AES. [b] The real number of Sn equivalents were calculated considering the number of Pt and Sn moles obtained from ICP-AES analysis. [c] The number of Sn equivalents were calculated considering the results obtained from STEM-EDX. [d] % of Pt surface atoms were estimated by using the NP size and the atom's magic number approach (*ChemCatChem* 2011, **3**, 1413-1418).

S4. TEM images

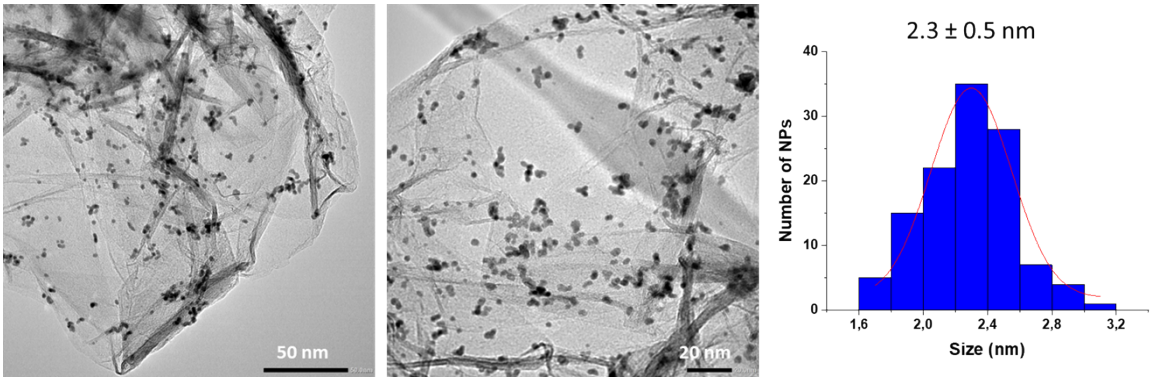

Figure S2. TEM image and size distribution histogram of **Pt@rGO/$Sn_{0.2}$**.

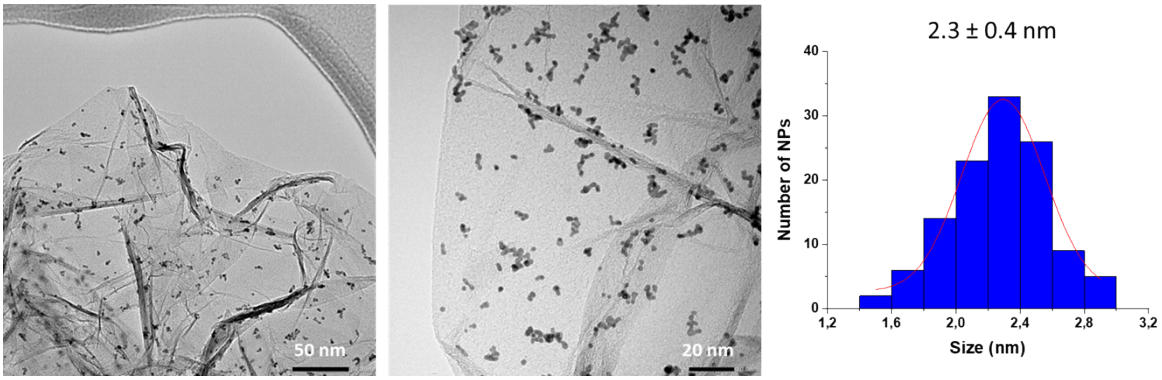

Figure S3. TEM image and size distribution histogram of **Pt@rGO/$Sn_{0.5}$**.

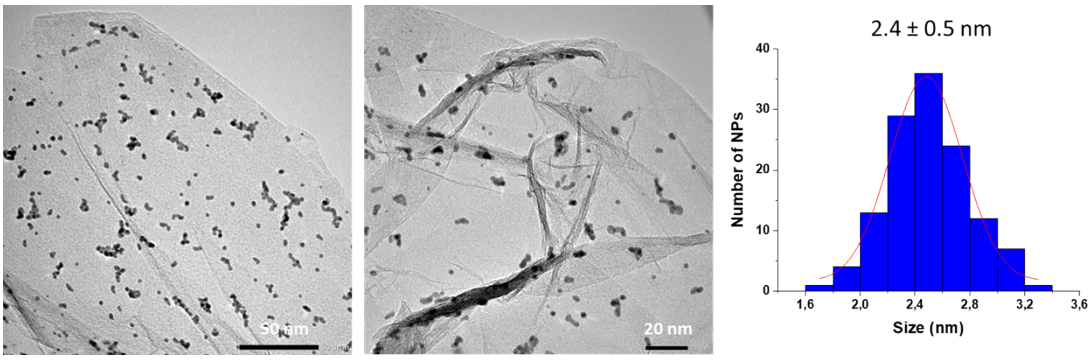

Figure S4. TEM image and size distribution histogram of **Pt@rGO/Sn$_1$**.

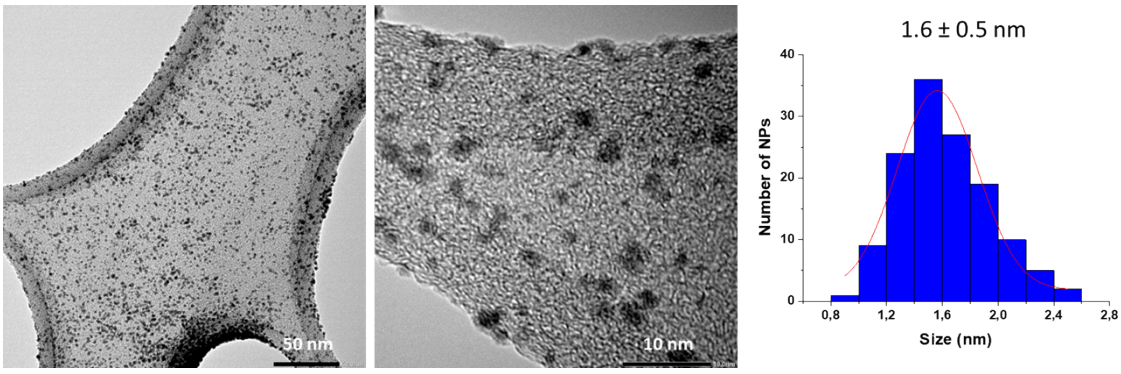

Figure S5. TEM image and size distribution histogram of **Pt/Sn$_2$**.

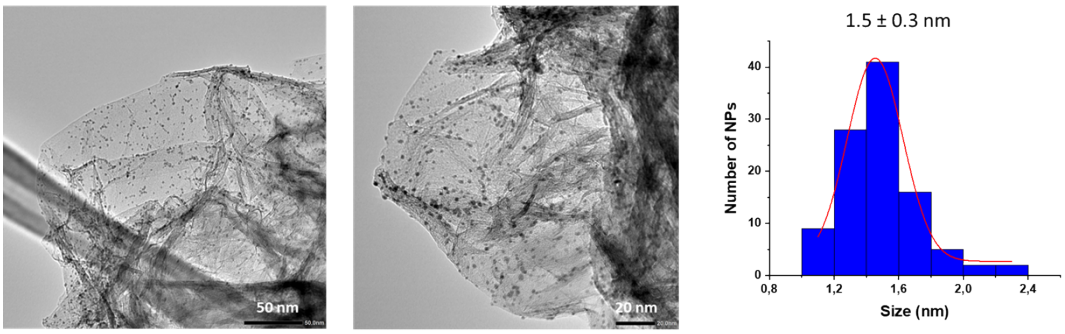

Figure S6. TEM image and size distribution histogram of **Pt/Sn$_2$@rGO**.

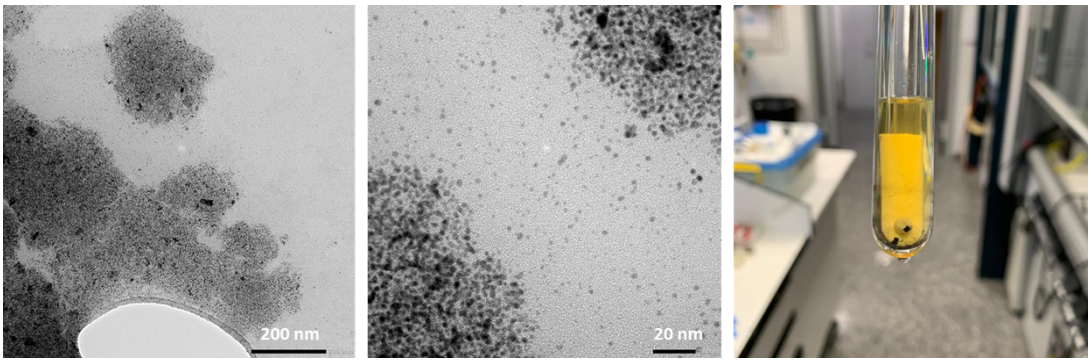

Figure S7. TEM and macroscopic images of **Pt/Sn$_2$** after hydrogenation of HMF. Conditions: 0.1 mol% **Pt/Sn$_2$**, H_2O (2 mL), H_2 (5 bar), 25 ºC, 5 h.

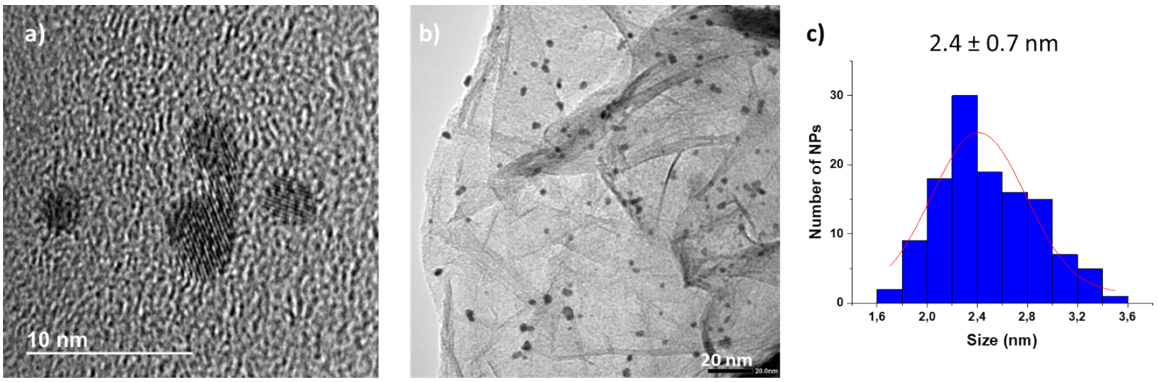

Figure S8. HRTEM (a) and TEM (b) images with the corresponding size histogram (c) of **Pt@rGO** after hydrogenation of HMF. Conditions: HMF (0.3 mmol), H_2O (2 mL), H_2 (5 bar), 25 ºC, 5 h.

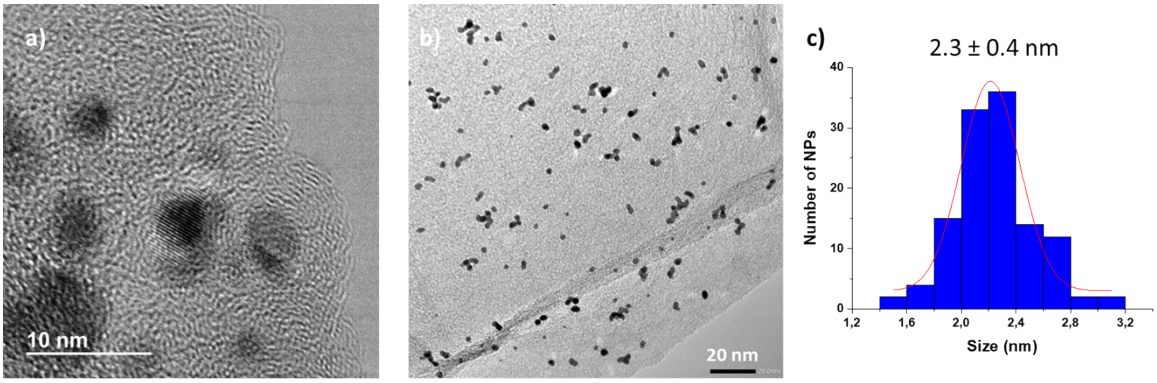

Figure S9. HRTEM (a) and TEM (b) images with the corresponding size histogram (c) of **Pt@rGO/$Sn_{0.8}$** after hydrogenation of HMF. Conditions: HMF (0.3 mmol), H_2O (2 mL), H_2 (5 bar), 25 ºC, 5 h.

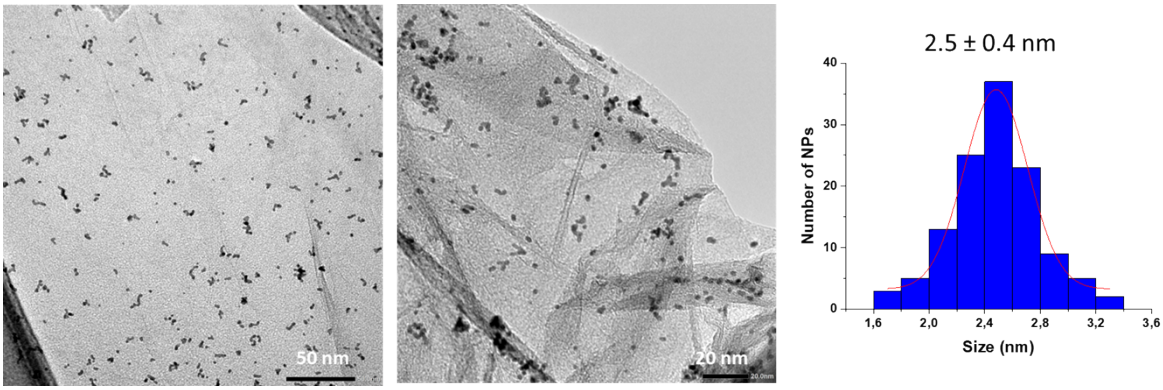

Figure S10. TEM images and size histogram of **Pt@rGO/$Sn_{0.8}$** after multiple addition experiment.

S5. HRTEM and STEM images

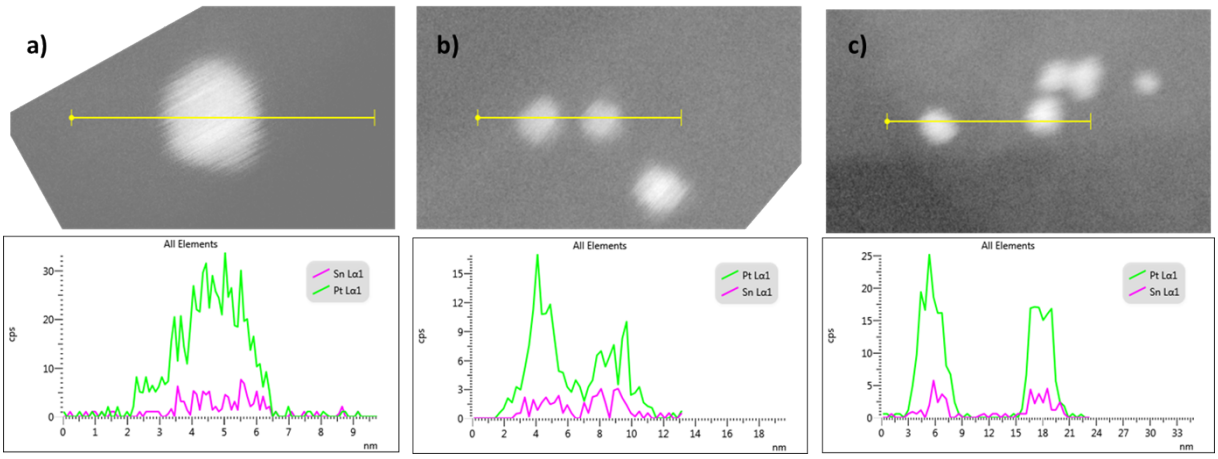

Figure S11. HAADF-STEM images and relative composition profiles of (a) **Pt@rGO/Sn$_{0.2}$** (b) **Pt@rGO/Sn$_{0.5}$** and (c) **Pt@rGO/Sn$_1$** determined by EDX.

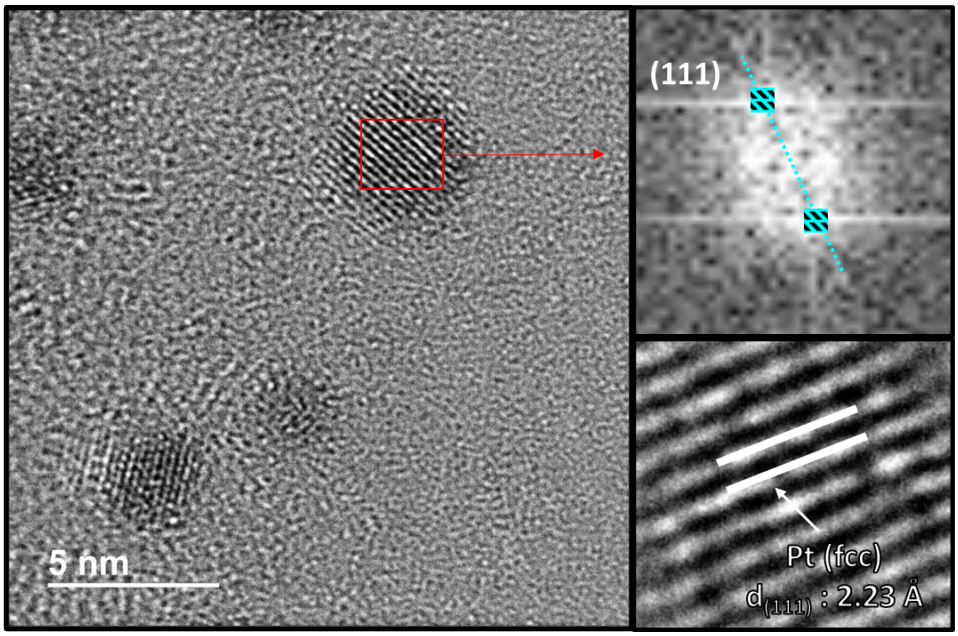

Figure S12. HRTEM micrographs of **Pt/Sn$_2$** (left, right bottom) and Fourier Transform Analysis with the planar reflections (right, top), which displays reflection to the (111) atomic plane, and chosen expanded zone (right, bottom) showing a lattice fringe spacing of 2.23 Å.

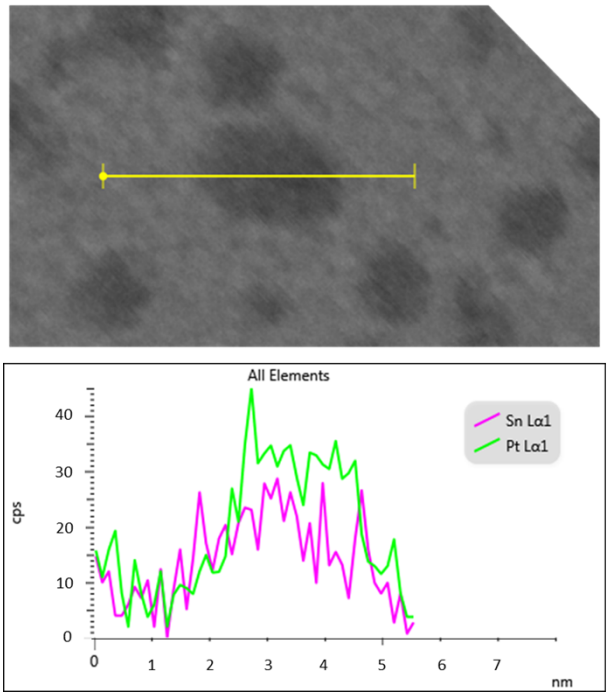

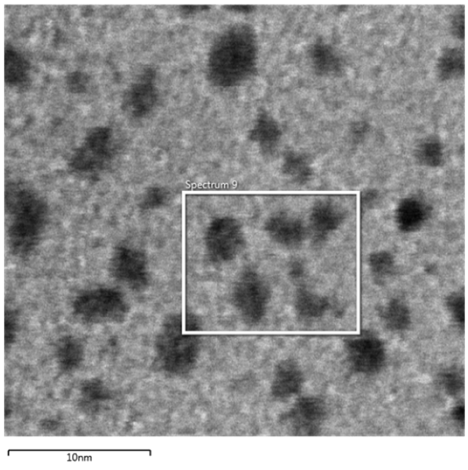

Catalyst	Pt wt%	Sn wt%	n_{eq} Sn EDX	n_{eq} Sn[a] ICP
Pt/Sn_2	49.2	34.7	1.01	1.15

Figure S13. HAABF-STEM images and relative composition profile of **Pt/Sn_2** determined by EDX.

S6. RAMAN

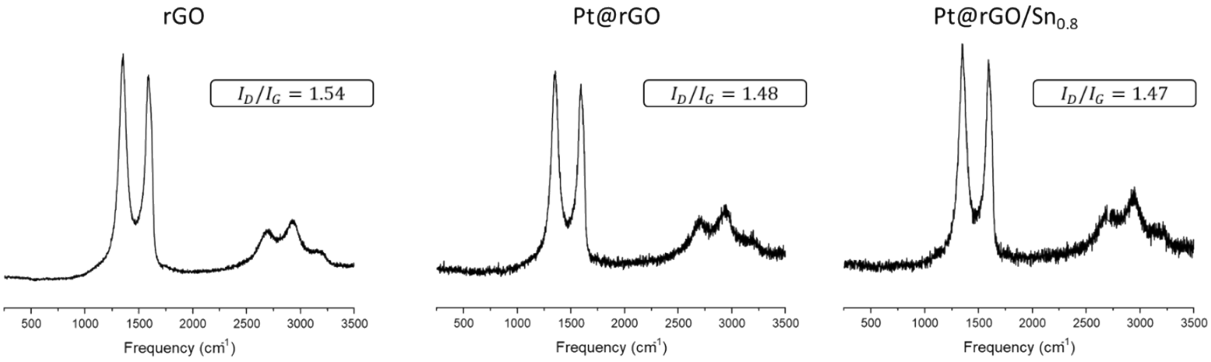

Figure S14. Raman spectrum and I_D/I_G ratio of rGO, **Pt@rGO** and **$Pt@rGO/Sn_{0.8}$**.

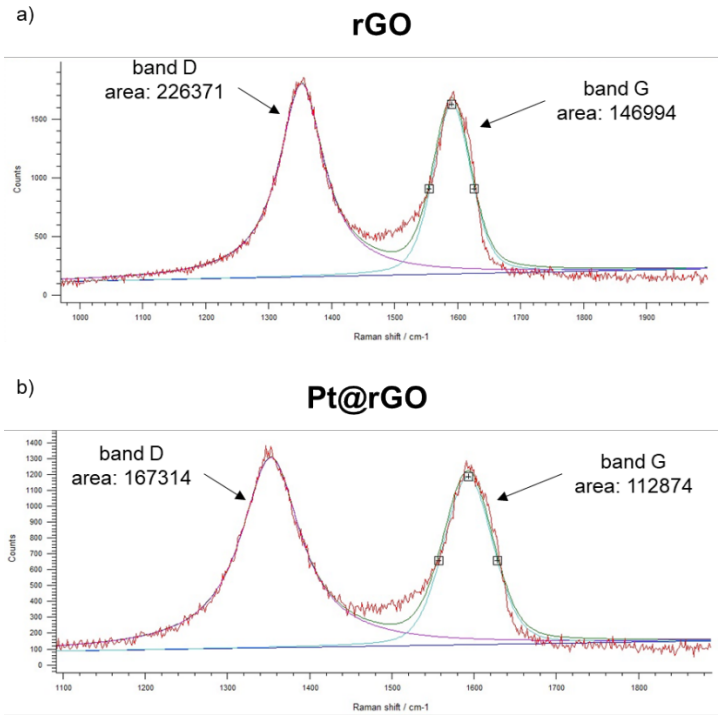

Figure S15. Deconvolution of Raman spectra of (a) rGO and (b) **Pt@rGO**.

S7. DRIFT

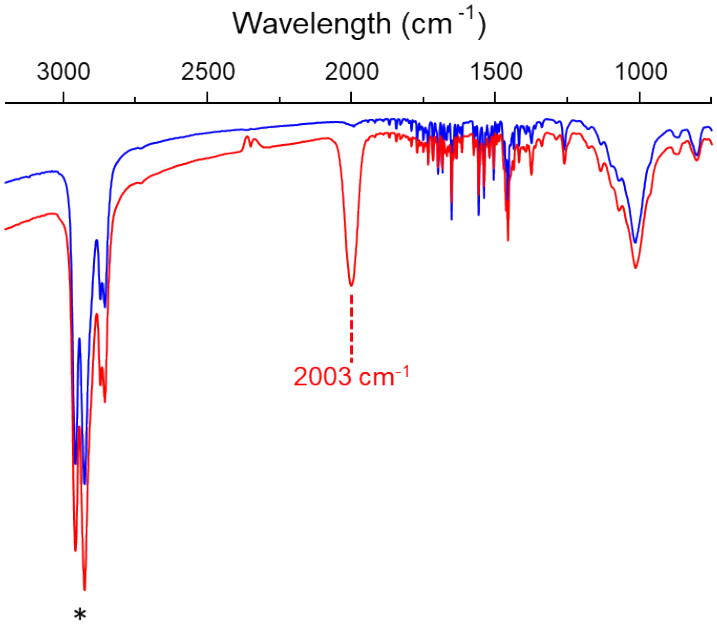

Figure S16. DRIFT spectra of **Pt/Sn_2** before (blue) and after (red) CO adsorption (bubbling CO into a THF dispersion during 5 min). The bands with asterisk correspond to THF.

S8. XPS

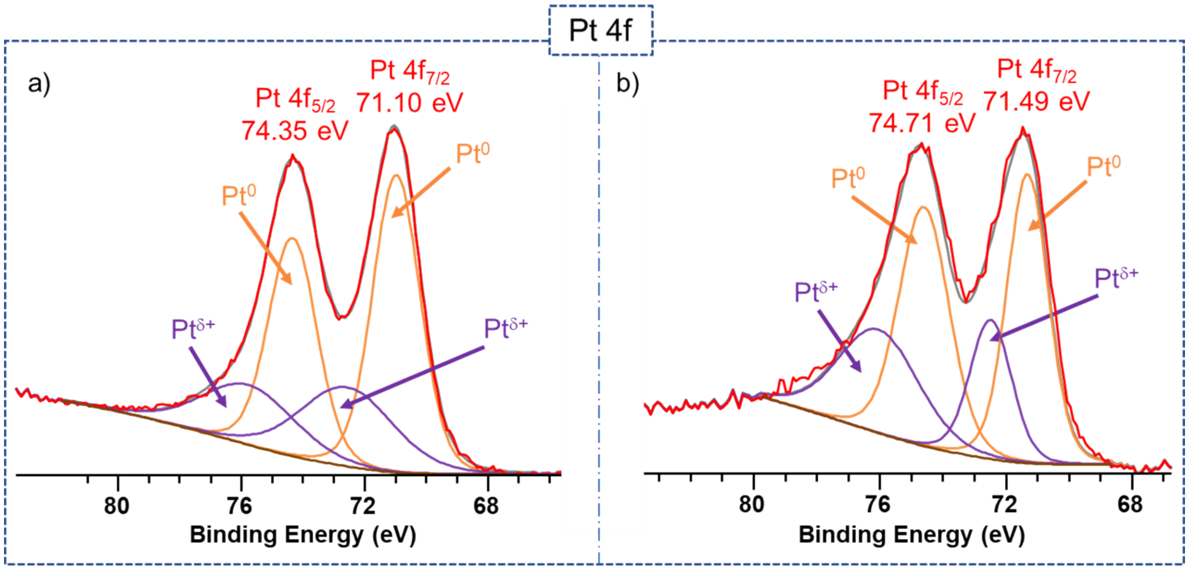

Figure S17. XPS of Pt 4f areas of (a) **Pt/Sn₂** and (b) **Pt@rGO**.

S9. X-ray powder diffraction (XRD)

Figure S18 mainly shows two broad peaks, a first one located at ca. 20°, which is associated to the Kapton foil used during the analysis under inert atmosphere; and another centred at *ca.* 40º, which is attributed to fcc-Pt and confirms that Pt NPs are predominantly as Pt^0. Due to the small size of the NPs (1.6 ± 0.5 nm observed by TEM) the signal is very broad. In any case, knowing the values of 2θ and FWHM (width at half height) of the peak, it was possible to approximately determine the size of the nanocrystal through the Scherrer equation (crystallite-size = (k·λ)/(β·cosθ)). Thus, applying this equation to our signal (FWHM of 8.723°) the crystallite size of **Pt/Sn_2** is approximately 1.2 nm, which agrees with TEM analysis.

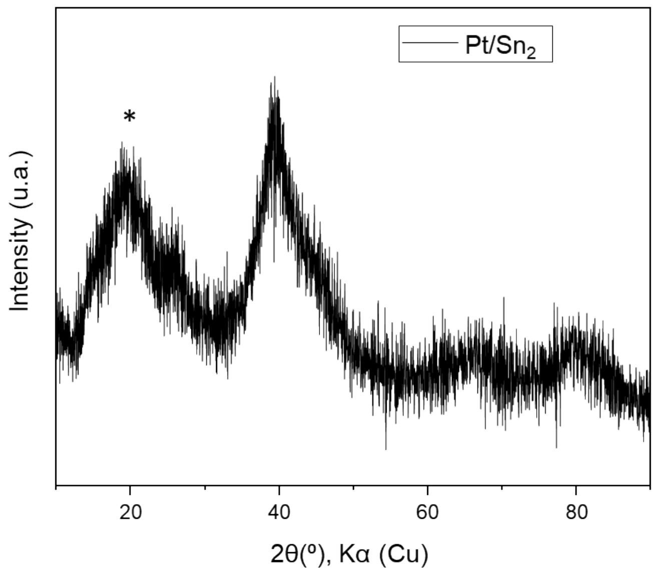

S10.

Figure S18. XRD diffractogram of **Pt/Sn_2**. The peak with asterisk corresponds to Kapton foil.

On the other hand, **Pt@rGO/Sn$_{0.8}$** XRD pattern do not show any significant peak associated to Pt, due to the low metal content and the small size of these supported NPs (~ 2 nm).

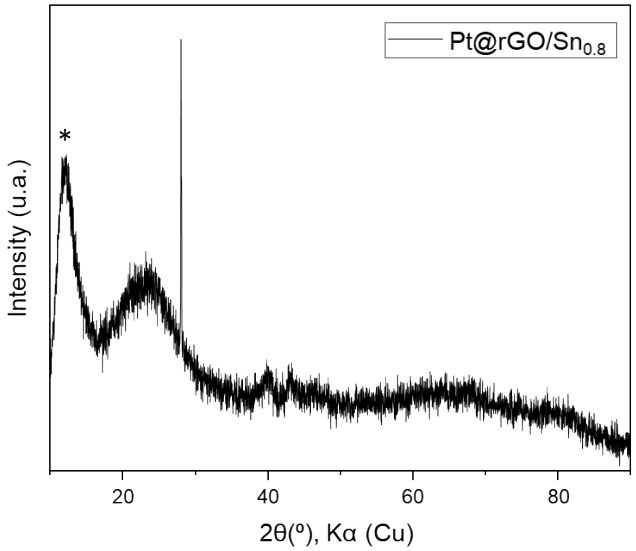

S11.

Figure S19. XRD diffractogram of **Pt@rGO/Sn$_{0.8}$**. The peak with asterisk corresponds to grease.

S.10 Solid-state NMR

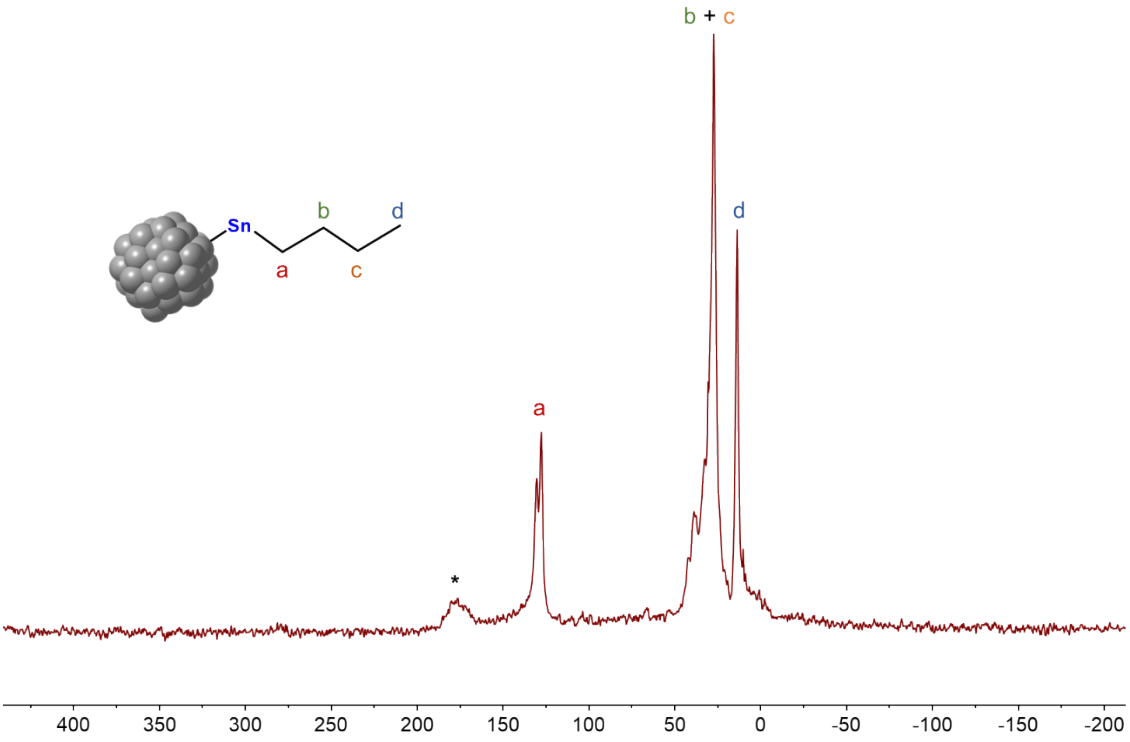

Figure S20. ^{13}C CP-MAS NMR spectra of **Pt/Sn$_2$**. The peak with asterisk corresponds to a spinning side band.

S.11 Catalytic Studies

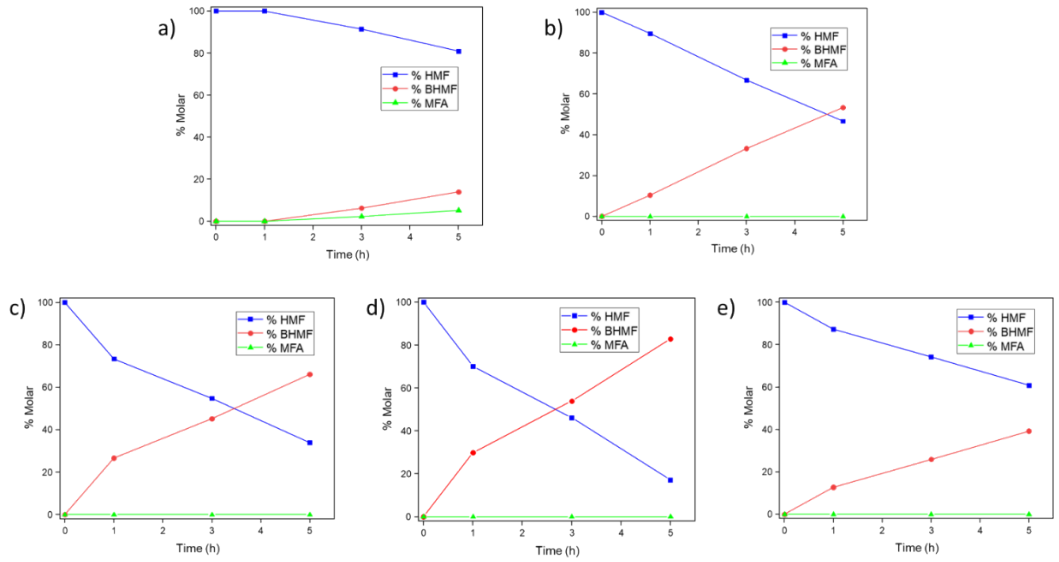

Figure S21. Hydrogenation of HMF in THF using (a) **Pt@rGO**, (b) **Pt@rGO/Sn$_{0.2}$**, (c) **Pt@rGO/Sn$_{0.5}$**, (d) **Pt@rGO/Sn$_{0.8}$** and (e) **Pt@rGO/Sn$_{1}$** as catalysts. Reaction conditions: 0.2 mmol HMF, 2 mg **Pt@rGO/Sn$_{x}$** (0.15 mol% Pt), 2 mL THF, 5 bar H_2, 25 ºC. Conversions and selectivities were determined by GC using dodecane as internal standard, and confirmed by GC-MS.

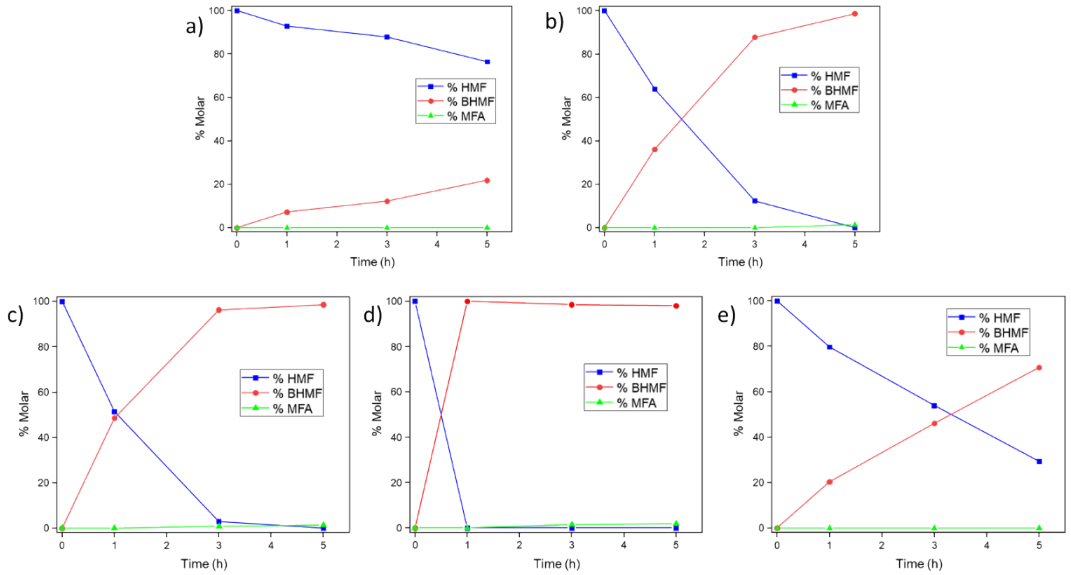

Figure S22. Hydrogenation of HMF in H_2O using (a) **Pt@rGO**, (b) **Pt@rGO/Sn$_{0.2}$**, (c) **Pt@rGO/Sn$_{0.5}$**, (d) **Pt@rGO/Sn$_{0.8}$** and (e) **Pt@rGO/Sn$_{1}$** as catalysts. Reaction conditions: 0.2 mmol HMF, 2 mg **Pt@rGO/Sn$_{x}$** (0.15 mol% Pt), 2 mL H_2O, 5 bar H_2, 25 ºC. Conversions and selectivities were determined by GC using dodecane as internal standard, and confirmed by GC-MS.

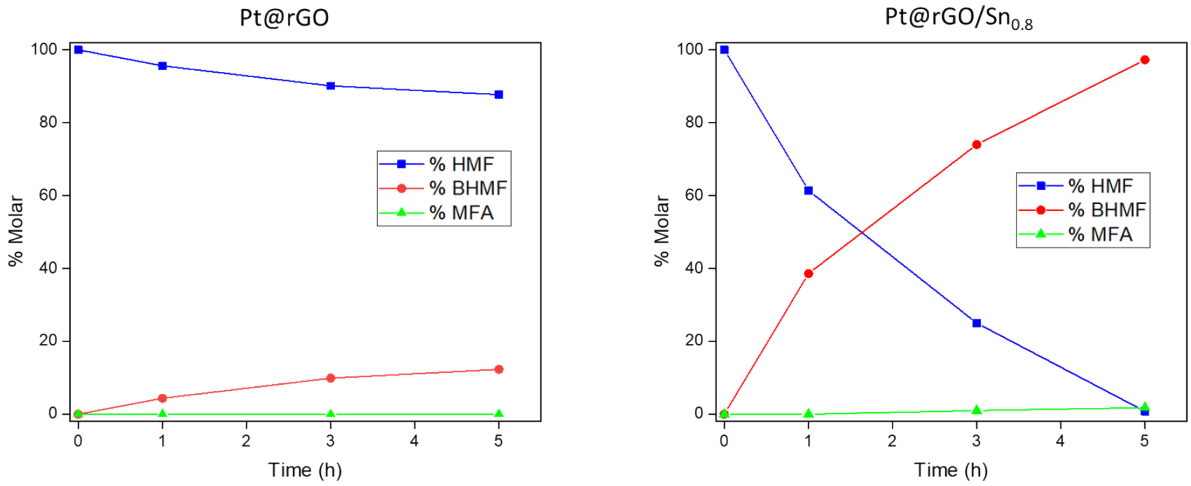

Figure S23. Hydrogenation of HMF in water using **Pt@rGO** (left) and **Pt@rGO/Sn$_{0.8}$** (right) as catalysts. Reaction conditions: 0.3 mmol HMF, 2 mg **Pt@rGO/Sn$_x$** (0.1 mol% Pt), 2 mL H_2O, 5 bar H_2, 25 ºC. Conversions and selectivities were determined by GC using dodecane as internal standard, and confirmed by GC-MS.

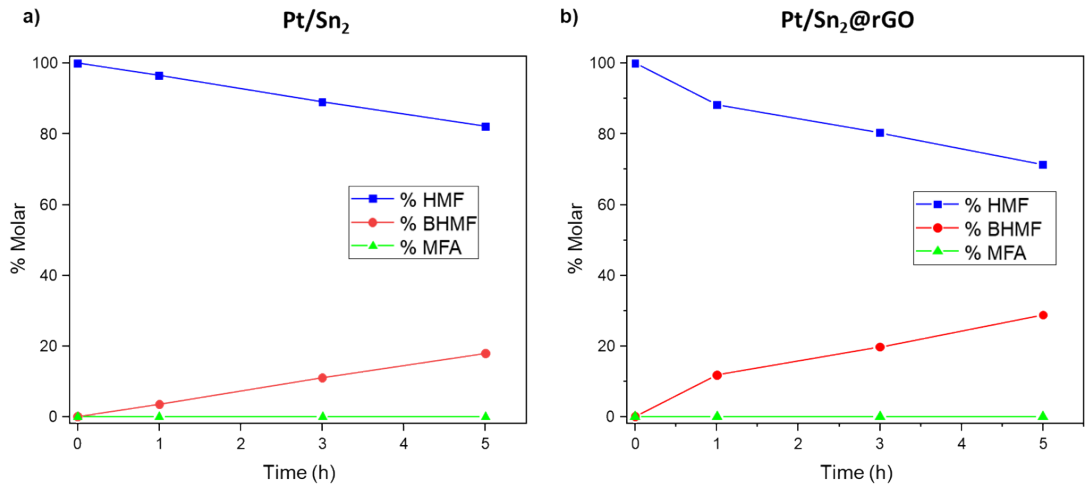

Figure S24. Hydrogenation of HMF in H_2O using (a) colloidal **Pt/Sn$_2$** and (b) supported **Pt/Sn$_2$@rGO** as catalyst. Reaction conditions: 0.3 mmol HMF, 0.1 mol% Pt, 2 mL H_2O, 5 bar H_2, 25 ºC. Conversions and selectivities were determined by GC using dodecane as internal standard, and confirmed by GC-MS.

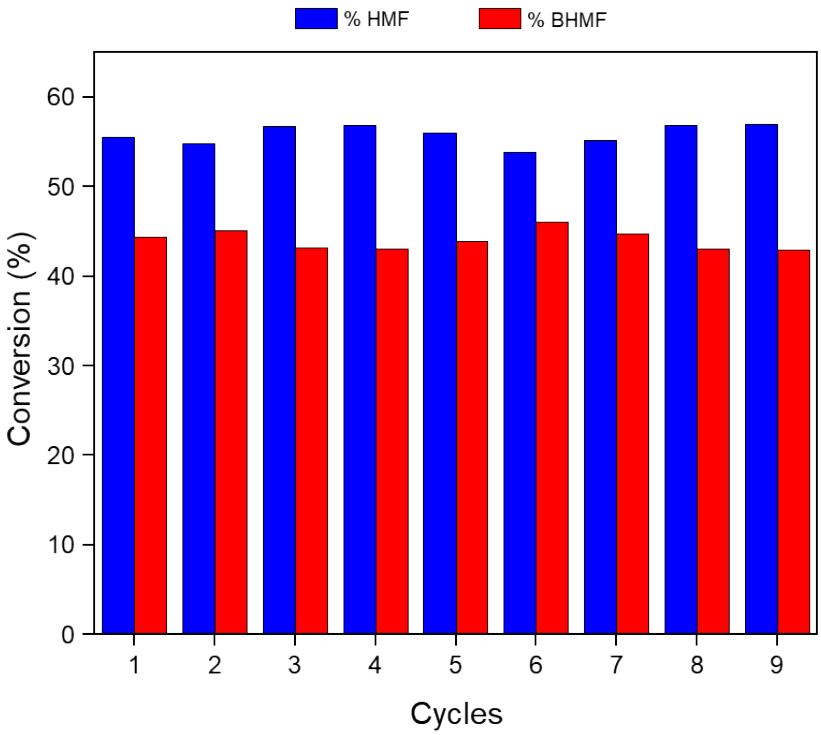

Figure S25. Multiple addition experiment for the hydrogenation of HMF catalyzed by **Pt@rGO/Sn$_{0.8}$**. Reaction conditions: 0.3 mmol HMF, 2 mg **Pt@rGO/Sn$_{0.8}$** (0.1 mol% Pt), 2 mL H_2O, 5 bar H_2, 25 ºC. Conversions and selectivities were determined by GC using dodecane as internal standard, and confirmed by GC-MS.

S12. State-of-the-art catalysts for the reduction of HMF

Table S3. State-of-the-art catalysts for the selective hydrogenation of HMF to BHMF.

Entry	Catalyst	Catalyst/HMF (mol %)	Solvent	Temp.	H_2 (bar)	Time (h)	Conversion (%)	TOF (h^{-1})[a]	BHMF yield (%)	Ref.
1	$PtSn/Al_2O_3$ (1 wt%)	0.25	ethanol	60	14	5	90	72	82	*4*
2	Pt/MCM-41 (1 wt%)	0.15	H_2O	35	8	1	85	566.7	95	*5*
3	Pt/Y (1 wt%)	1	H_2O	80	20	4	>99	25	100	*6*
4	Pt/CeO_2-ZrO_2 (1 wt%)	0.7	EtOH	20	1	2	95	67.9	100	*7*
5	Pt/C (5 wt%)	0.63	H_2O	140	70	1	64.5	102.4	10.7	*8*
6	Ru/MSN-Zr (5 wt%)	3	H_2O	25	5	4	98.1	8.2	90.3	*9*
7	$Ru/MnCo_2O_4$ (4 wt%)	2	methanol	100	82	4	>99	12.5	98	*10*
8	Ru/MgO-ZrO_2 (1 wt%)	0.2	1-butanol/H_2O	130	28	2	99	247.5	94	*11*
9	Ru/PMF	1	H_2O	50	20	8	90	11.2	89.1	*12*
10	Cu/SiO_2 (56 wt%)	11.2	methanol	100	25	8	100	1.1	97	*13*
11	$Cu/MgAlO_x$ (17 wt%)	7.8	1,4-dioxane	180	15	5	97.3	2.5	95.3	*14*
12	Cu@C-POP (10 wt%)	4.7	ethanol	50	20	8	95	2.5	95	*7*
13	Au/Al_2O_4 (1 wt%)	0.25	H_2O	120	65	2	100	200	96	*15*
14	$Au/FeO_x/Al_2O_3$ (1 wt%)	0.25	H_2O	80	3	2	96	192	96	*16*
15	Ni/Al_2O_3 (47 wt%)	14	H_2O	80	20	6	>99	1.2	25	*17*
16	$Pt@rGO/Sn_{0.8}$ (3 wt%)	0.15	H_2O	25	5	1	>99	666.7	100	***This work***

[a] Turn over frequencies (TOFs) were calculated considering the number of moles of HMF consumed and the number of moles of metal per time as previously reported.[18]

S13. CO and H_2 chemisorption experiments

Table S4. H_2 and CO chemisorption of **Pt@rGO** and **Pt@rGO/Sn$_{0.8}$**.

Catalyst	H_2 uptake ($\mu mol/g_{cat}$)	Crystal size (nm)	Dispersion	CO uptake ($\mu mol/g_{cat}$)
Pt@rGO	50.0	1.74	65.1	6.4
Pt@rGO/Sn$_{0.8}$	50.8	1.72	66.0	9.6

S14. Temperature-programmed reduction (TPR)

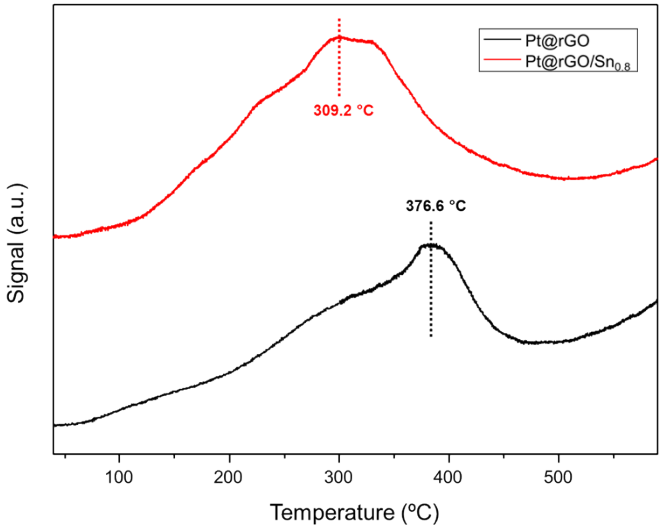

Figure S26. TPR profiles of **Pt@rGO** (black) and **Pt@rGO/Sn$_{0.8}$** (red).

S15. Hydrogen temperature-programmed desorption (H_2-TPD)

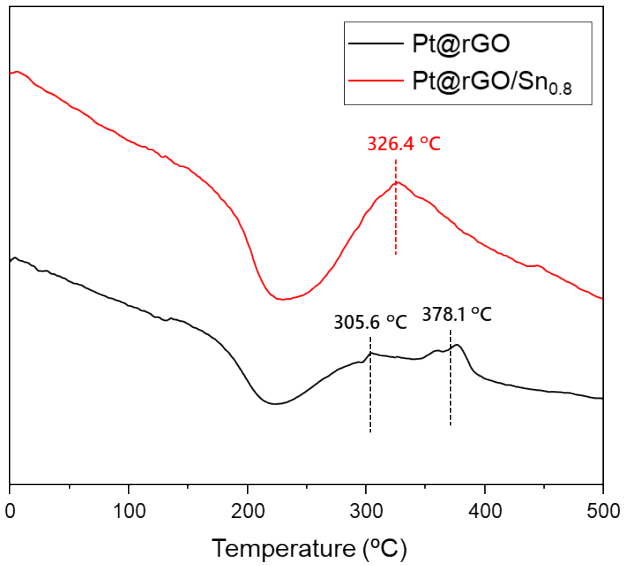

Figure S27. H_2-TPD patterns of **Pt@rGO** (black) and **Pt@rGO/Sn$_{0.8}$** (red).

S16. UV-vis spectra

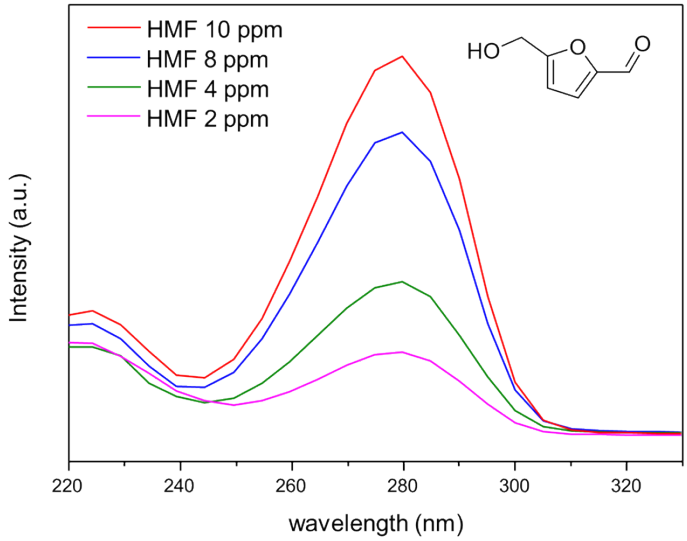

Figure S28. UV-vis calibration curves of HMF at different concentrations (10, 8, 4 and 2 ppm).

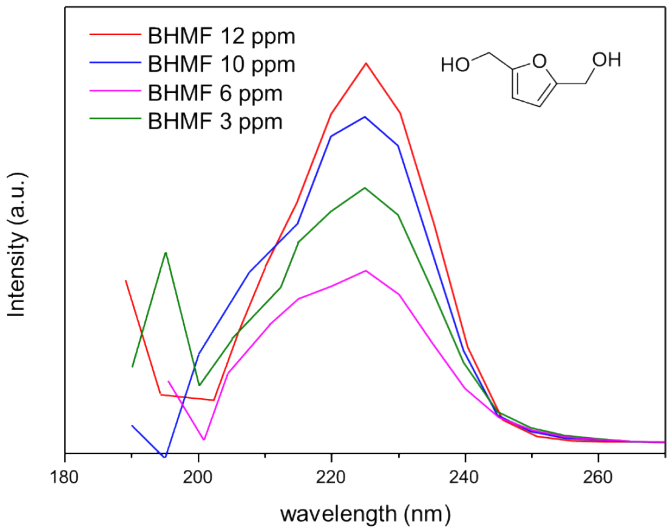

Figure S29. UV-vis calibration curves of BHMF at different concentrations (12, 10, 6 and 3 ppm).

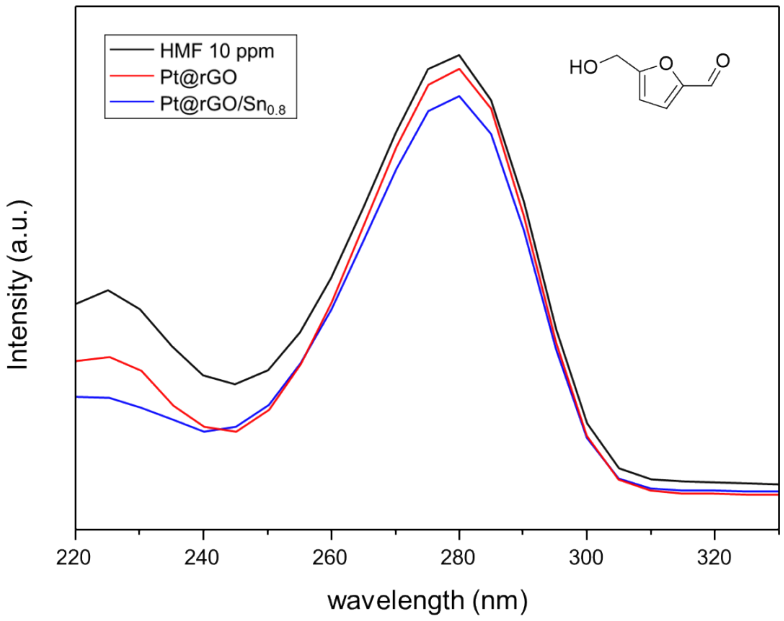

Figure S30. UV-vis spectra of the solutions after adsorption of HMF by **Pt@rGO** (red) and **Pt@rGO/Sn$_{0.8}$** (blue).

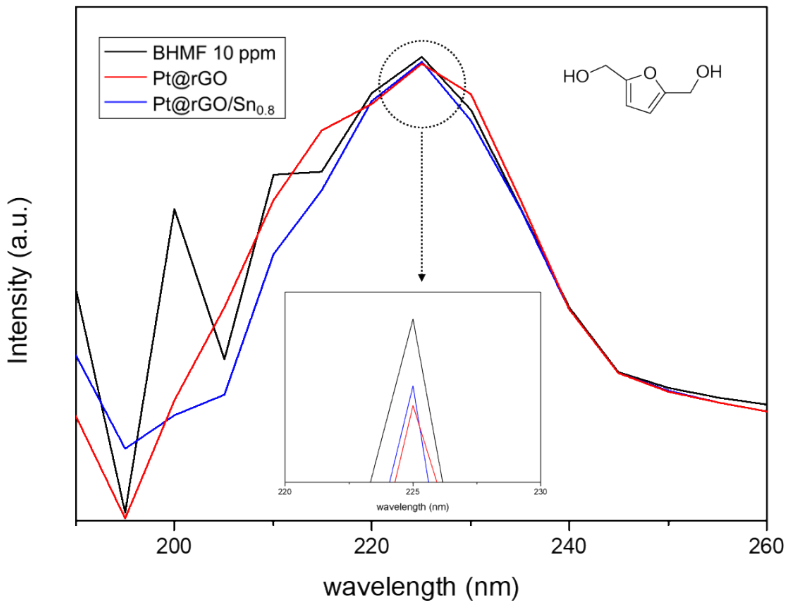

Figure S31. UV-vis spectra of the solutions after adsorption of BHMF by **Pt@rGO** (red) and **Pt@rGO/Sn$_{0.8}$** (blue).

References

1. L. M. Martínez-Prieto, M. Puche, C. Cerezo-Navarrete and B. Chaudret. Uniform Ru nanoparticles on N-doped graphene for selective hydrogenation of fatty acids to alcohols. *J. Catal.*, 2019, **377**, 429-437.

2. F. Humblot, D. Didillon, F. Lepeltier, J. P. Candy, J. Corker, O. Clause, F. Bayard and J. M. Baset. Surface Organometallic Chemistry on Metals: Formation of a Stable Sn(*n*-C_4H_9) Fragment as a Precursor of Surface Alloy Obtained by Stepwise Hydrogenolysis of Sn(*n*-C_4H_9)$_4$ on a Platinum Particle Supported on Silica. *J. Am. Chem. Soc.,* 1998, **120**, 137-146.

3. C. Cerezo-Navarrete, Y. Mathieu, M. Puche, C. Morales, P. Concepción, L. M. Martínez-Prieto and A. Corma. Controlling the selectivity of bimetallic platinum.ruthenium nanoparticles supported on N-doped graphene by adjusting their metal composition. *Catal. Sci. Technol.*, 2021, **11**, 494–505.

4. M. Balakrishnan, E. R. Sacia and A. T. Bell. Etherification and reductive etherification of 5-(hydroxymethyl)furfural: 5-(alkoxymethyl)furfurals and 2,5-bis(alkoxymethyl)furans as potential bio-diesel candidates. *Green Chem.,* 2012, **14**, 1626-1634.

5. M. Chatterjee, T. Ishizaka and H. Kawanami. Selective hydrogenation of 5-hydroxymethylfurfural to 2,5-bis(hydroxymethyl)furan using Pt/MCM-41 in an aqueous medium: a simple approach. *Green Chem.,* 2014, **16**, 4734-4739.

6. Q. Chen, T. Li, Y. Zhou, Y. Bi, S. Guo, X. Liu, H. Kang, M. Wang, L. Liu, E. Xing and D. Yang. Selective Hydrogenation of 5-Hydroxymethylfurfural via Zeolite Encapsulation to Avoid Further Hydrodehydroxylation. *Ind. Eng. Chem. Res.,* 2020, **59**, 12004-12012.

7. Y. Wang, H. Wang, X. Kong and Y. Zhu. Catalytic Conversion of 5-Hydroxymethylfurfural to High-Value Derivatives by Selective Activation of C-O, C=O, and C=C Bonds. *ChemSusChem* 2022, **15**, e202200421.

8. S. Fulignati, C. Antonetti, D. Licursi, M. Pieraccioni, E. Wilbers, H. J. Heeres and A. M. R. Galletti. Insight into the hydrogenation of pure and crude HMF to furan diols using Ru/C as catalyst. *Appl. Catal. A* 2019, **578**, 122-133.

9. J. Chen, F. Lu, J. Zhang, W. Yu, F. Wang, J. Gao and J. Xu. Immobilized Ru Clusters in Nanosized Mesoporous Zirconium Silica for the Aqueous Hydrogenation of Furan Derivatives at Room Temperature. *ChemCatChem* 2013, **5**, 2822-2826.

10. D. K. Mishra, H. J. Lee, C. C. Truong, J. Kim, Y.W. Suh, J. Baek and Y. J. Kim. Ru/$MnCo_2O_4$ as a catalyst for tunable synthesis of 2,5-bis(hydroxymethyl)furan or 2,5-bis(hydroxymethyl)tetrahydrofuran from hydrogenation of 5-hydroxymethylfurfural. *Mol. Catal.,* 2020, **484**, 110722.

11. R. Alamillo, M. Tucker, M. Chia, Y. Pagán-Torres and J. Dumesic. The selective hydrogenation of biomass-derived 5-hydroxymethylfurfural using heterogeneous catalysts. *Green Chem.,* 2012, **14**, 1413-1419.

12. M. Mani, G. G. Kadam, L. J. Konwar and A. B. Panda. Ru-supported mesoporous melamine polymers as efficient catalysts for selective hydrogenation of aqueous 5-hydroxymethylfurfural to 2,5-bis-/hydroxymethyl)furan. *Biomass Convers. Biorefinery* 2022.

13. Q. Cao, W. Liang, J. Guan, L. Wang, Q. Qu, X. Zhang, X. Wang and X. Mu. Catalytic synthesis of 2,5-bis-methoxymethylfuran: A promising cetane number improver for diesel. *Appl. Catal. A* 2014, **481**, 49-53.

14. C. Sarkar, R. Paul, S. C. Shit, Q. T. Trinh, P. Koley, B. S. Rao, A. M. Beale, C.W. Pao, A. Banerjee and J. Mondal. Navigating Copper-Atom-Pair Structural Effect inside a Porous Organic Polymer Cavity for Selective Hydrogenation of Biomass-Derived 5-Hydroxymethylfurfural. *ACS Sustainable Chem. Eng.,* 2021, **9**, 2136-2151.

15. J. Ohyama, A. Esaki, Y. Yamamoto, S. Arai and A. Satsuma. Selective hydrogenation of 2-hydroxymethyl-5-furfural to 2,5-bis(hydroxymethyl)furan over gold sub-nano clusters. *RSC Adv.,* 2013, **3**, 1033-1036.

16. J. Ohyama, Y. Hayashi, K. Ueda, Y. Yamamoto, S. Arai and A. Satsuma. Effect of FeO_x Modification of Al_2O_3 on Its Supported Au Catalyst for Hydrogenation of 5-Hydroxymethylfurfural. *J. Phys. Chem. C* 2016, **120**, 15129-15136.

17. N. Perret, A. Grigoropoulos, M. Zanella, T. D. Manning, J. B. Claridge and M. J. Rosseinsky. Catalytic Response and Stability of Nickel/Alumina for the Hydrogenation of 5-Hydroxymethylfurfural in Water. *ChemSusChem* 2016, **9**, 521-531.

18. A. P. Umpierre, E. de Jesús and J. Dupont. *Turnover Numbers and Soluble Metal Nanoparticles. ChemCatChem* 2011, **3**, 1413-1418.